



Demonstration of broadband magnetic polymer composite absorber crossing S- and C-bands

Linbo Zhang¹ · Jing Fan¹ · Yueyang Liu¹ · Haiyan Xie¹ · Jianliang Xie¹

Received: 11 June 2019 / Accepted: 11 March 2020 / Published online: 23 March 2020
© Springer-Verlag GmbH Germany, part of Springer Nature 2020

Abstract

In this paper, an ultra-thin microwave absorber with cross-resonator (CR) exhibiting a broad absorption bandwidth is designed and fabricated. Theoretical and experimental results show that the absorber has a wideband strong absorption in a frequency range from 2.2 to 6.8 GHz and from 2.2 to 5.4 GHz when incident electric field is *y*- and *x*-polarized, respectively. The equivalent *L*–*C* circuit and energy loss density clarify the mechanism underlying observed absorption. Moreover, the oblique incidence performance of the proposed absorber is also analyzed and shows that the broad bandwidth can be maintained as incident angle increases up to 30 degrees for *y*-polarized wave and 60 degrees for *x*-polarized wave, respectively. And when incident angle is fixed at 30 degrees the absorption bandwidth can be achieved from 2.1 to 7.5 GHz with azimuth angle of 90 degrees for *x*-polarized wave.

1 Introduction

Microwave absorber has continuously attracted enormous interest due to its widespread applications for prominent examples including electromagnetic (EM) interference, compatibility and stealth technology [1–6]. In 2008, Landy et al. [1] firstly reported perfect metamaterial absorber, which soon inspired the development of microwave absorbers [7,

8]. With the development of detective technology, improvement of low-frequency microwave absorption performance has been particularly important. Traditional microwave absorbers at low frequency are usually carried out based on a dielectric substrate [9–11]. However, the alignment involved in such a design would make its fabrication process complicated and challenging. Large thickness is also needed for these absorbers to expand the limited bandwidth.

Recently, attempts have been made to improve low-frequency absorbing properties with magnetic elements [12–20]. In Ref. [15], a magnetic-type absorber (MA) based on cross resonator (CR) was realized for exhibiting a – 10 dB bandwidth from 1.67 to 3.7 GHz with a total thickness of 2.42 mm. A second-order cross fractal metamaterial structure for such purpose was proposed in Ref. [17]. Chen et al. presented a multilayer MA to extend low-frequency absorption bandwidth [12]. However, the working bandwidth depends on operation frequency and suffers from narrow bandwidth, which may impede their applications. In previous papers, Zhang et al. [14] have designed a needle-shaped MA to improve the low-frequency properties, and the bandwidth could be extended with a relatively thinner thickness. In Refs. [7] and [15], the physics mechanisms of these cross-shaped absorbers can be explained by the destructive interference and equivalent circuit model. These two intriguing features, therefore, make it possible for us to design a simple MA in both S and C frequency regimes.

Electronic supplementary material The online version of this article (<https://doi.org/10.1007/s00340-020-7415-5>) contains supplementary material, which is available to authorized users.

✉ Linbo Zhang
zlbyeah0806@126.com

Jing Fan
fjffj@163.com

Yueyang Liu
yyluiyueyang@163.com

Haiyan Xie
uestchaiyan@163.com

Jianliang Xie
jlx@uestc.edu.cn

¹ State Key Laboratory of Electronic Thin Film and Integrated Devices, National Engineering Research Center of Electromagnetic Radiation Control Materials and University of Electronic Science and Technology of China, Shahe Campus: No. 4, Section 2, North Jianshe Road, Chengdu 610054, People's Republic of China

In this work, a facile approach is employed for achieving simultaneously ultra-thin and wideband microwave absorber using periodic CR pattern and magnetic polymer composite crossing *S*- and *C*-bands. Our proposed absorber exhibits wideband absorption properties demonstrated numerically as well as experimentally. Both the equivalent *L*–*C* resonant circuit and EM field analysis are proposed to explain the physical mechanism. Finally, the oblique incidence performance of the proposed absorber varying is also given.

2 Design and experiment

The schematic of the proposed MA is illustrated in Fig. 1a and b, which consists of arrays of CR pattern placed on top of a magnetic polymer composite with thickness $t = 2.0$ mm. The period of the unit cell is $a_x = 22$ mm, $a_y = 12$ mm, and the dimensions of the CR patterns are $l = 8.0$ mm, $w = 1.0$ mm and $t_n = 0.002$ mm. The magnetic polymer composite used throughout this work was prepared on the basis of epoxy resin filled with FeCo alloy powders at the weight ratio of 1:9 by blending, roll mixing, and vulcanizing [21, 22]. The complex EM parameters (as shown in Fig. 2) were measured by Agilent 8720ET vector network analyzer based on reflection/transmission technique by inserting the toroidal sample into a coaxial waveguide with the same inner and outer diameter as the sample. The EM parameters were derived from the scattering parameters (*S* parameters) based on the so-called Nicolson-Ross-Weir principle [23].

The finite-difference time-domain (FDTD) solver CST Microwave Studio software (Version 2014) was used to demonstrate the microwave absorption properties of our design. A single unit cell was simulated with appropriate boundary conditions, as unit cell in both *x* and *y* directions, and open (add space) in *z* direction. And under this periodic boundary condition, the Floquet mods are TE and TM modes. Under TE mode, electric and magnetic fields are along *y*- and *x*-axis, respectively. And under TM mode, electric and magnetic fields are along *x*- and *y*-axis, respectively. EM plane waves were incident on the surface of the structure. In simulations, the material type of the CA pattern

in simulations is lossy metal with electric conductivity of 3.72×10^7 S/m. we can obtain all the relationships between the reflection coefficient and the geometric dimensions. For experiments, the MA was fabricated in the form of rubber board; the copper film was pasted on the magnetic absorbing sheet with glue and the etched into arrays of CA pattern with the mechanical lithography method. The total area of the sample is 200×200 mm². An image of the fabricated MA is presented in Fig. 1c. Agilent 8720ET vector network analyzer connected to two standard gain broadband antennas was employed to measure the proposed MA in an EM anechoic chamber.

Figure 3 shows the simulated and measured reflection coefficients. Owing to the asymmetric of the diagonal of the unit cell, the proposed MA shows dependent on the direction of the incident electric field. When the incident electric field is *y*-polarized as shown in Fig. 3(a), two absorption peaks can be observed clearly at the frequencies of 2.5 GHz and 4.8 GHz for simulation and 2.9 GHz and 4.5 GHz for measurements, respectively. It can also be seen that the simulated absorption bandwidth is achieved from 2.1 to 6.8 GHz and from 2.2 to 6.8 GHz for measurements. As depicted in Fig. 3(b), when the incident electric

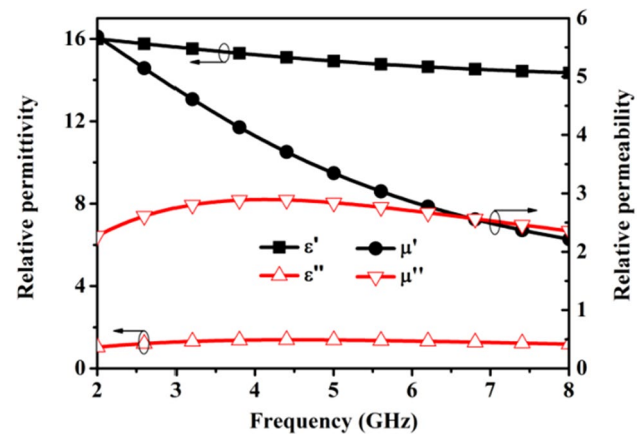
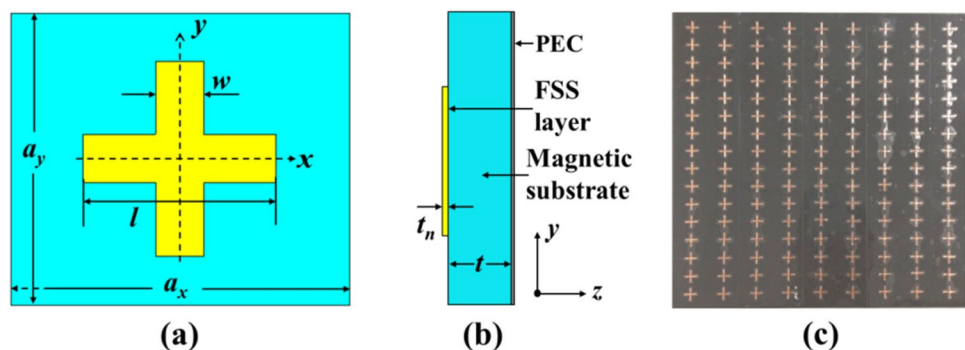


Fig. 2 Measured relative electromagnetic parameters of the magnetic absorbing material as a function of frequency

Fig. 1 **a** Front view of the unit cell, **b** cross-section schematic of the absorber, **c** the photography of the measured sample



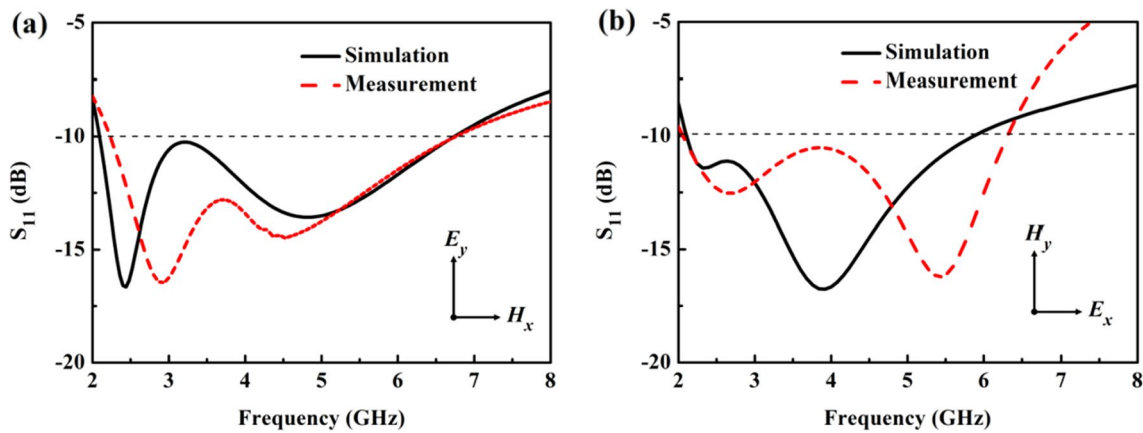


Fig. 3 Simulated and measured reflection coefficients for the proposed absorber with the incident electric field propagating along **a** *y*-polarized and **b** *x*-polarized

field is *x*-polarized, the resonant frequencies are 2.3 GHz, 3.9 GHz for simulation and 2.5 GHz, 4.1 GHz for measurement. The MA still exhibits broad absorption bandwidth from 2.2 to 5.8 GHz for simulation and from 2.2 to 5.4 GHz for measurement. However, there is a discrepancy between the simulated and measured results. Both the infinite sample size and actual EM parameters can affect the measured results. Meanwhile, the limited precision of fabrication geometry also affects the results. Despite of these discrepancies, the proposed MA is still able to sustain low-frequency broadband absorption property. Some recently reported broadband microwave absorbers at low frequency are summarized for comparison in Table 1. It is apparent that the proposed MA operates in a higher frequency range with a wider bandwidth. In addition, the thickness of the proposed MA requires only 2 mm.

3 Results and discussion

Figure 4 shows the simulated reflection coefficients of the proposed MA with different thickness. The absorption property is sensitive to the thickness. We can see that whenever the incident electric is *y*-or *x*-polarized, the two resonant frequencies gradually shift towards lower frequency as *t* increases. And then the high-frequency absorption peak gradually disappears and the absorption bandwidth becomes narrow. When the thickness is about 2 mm, the absorption bandwidth is widest. Due to the frequency-dispersive permeability of magnetic polymer composite, the design of ultrathin and broadband MA is more complicated compared with non-magnetic microwave absorber. As discussed in Refs. [15] and [16], the authors have introduced the effect of frequency selective surfaces (FSSs) on the absorption characteristics of MA. As a result, we will analyze the introduction

Table 1 The recent reported broadband microwaves absorbers at low-frequency microwave bands

Paper	Bandwidth (GHz)	Thickness (mm)	Substrate	Dependent on the direction of E_{in}^c
[8]	4–8	4.2	FR-4	No
[9]	2.2–9.5	4	FR-4 and Magnetic coatings	No
[14]	2.0–4.4	3	Magnetic materials	No
[15]	3.0–5.3	2.6	FR-4 and Magnetic materials	No
[17]	1.67–3.7	2.42	Magnetic materials	No
Present study	2.2–6.8 ^a 2.1–6.2 ^b	2	Magnetic materials	Yes

^aThe incident electric field is *y*-polarized

^bThe incident electric field is *x*-polarized

^c E_{in} represents the incident electric field

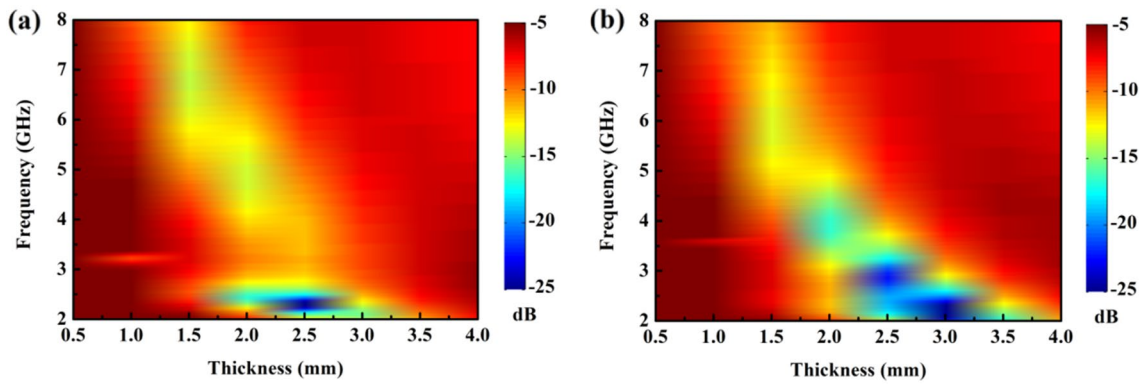


Fig. 4 Simulated reflection coefficients with different thickness t when the incident electric field is **a** y -polarized and **b** x -polarized

of CR on the absorption performance by equivalent circuit and energy loss density.

To make a better understanding of the characteristics of the proposed MA, we study the dependence of dimensional parameter a_x on the absorption properties when other parameters are fixed as illustrated in Fig. 5. First, when the incident electric field is y -polarized (see Fig. 5a), it is observed that two resonant peaks can be generated with

increases of a_x . When $a_x = 22$ mm, the -10 dB absorption bandwidth is achieved from 2.1 to 6.8 GHz. Second, the similar phenomenon occurs when the incident electric field is x -polarized as depicted in Fig. 5b. The -10 dB absorption bandwidth is 2.2 to 5.8 GHz when $a_x = 22$ mm. However, the low-frequency resonant peaks are gradually weaker with the increase of a_x both in these two cases. The phenomenon can be explained by an equivalent R - L - C parallel circuit

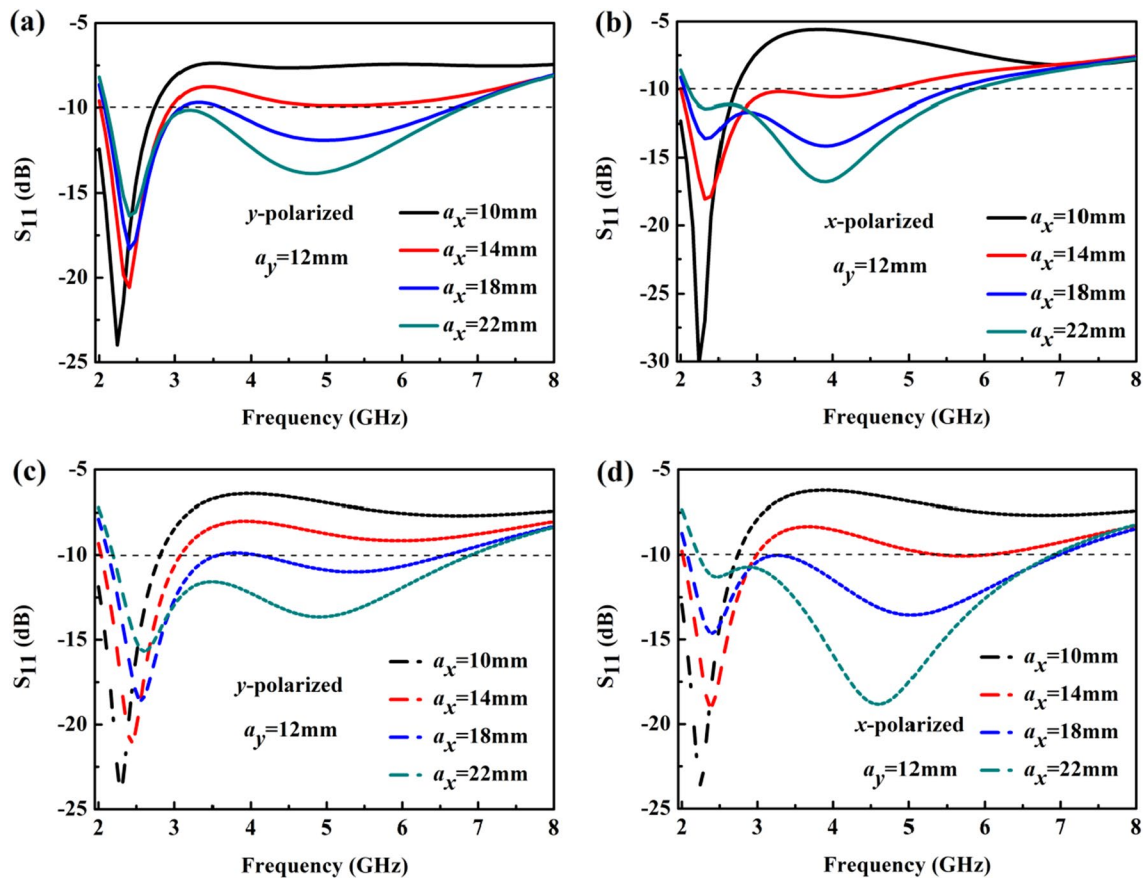


Fig. 5 Simulated (**a**, **b**) and calculated (**c**, **d**) reflection coefficient with different geometrical parameter a_x for the proposed MA

[13–15, 24–27]. The total capacitances C can be described approximately by a formula $C \approx lw\epsilon_0(\epsilon_r + 1)/(2a_x)$, and the total inductance L of the structure is approximately given by $L \approx a_x l \ln(t/w)\mu_0(\mu_r + 1)/2$. Thus the equivalent input impedance z_{in} and reflection coefficient S_{11} of the proposed MA can be expressed by:

$$z_d = iz_0 \sqrt{\frac{\mu_r}{\epsilon_r}} \tan\left(2\pi ft \frac{\sqrt{\mu_r \epsilon_r}}{c}\right) \tag{1}$$

$$z_{in} = \frac{\left(j2\pi fL + \frac{1}{j2\pi fC}\right)z_d}{j2\pi fL + \frac{1}{j2\pi fC} + z_d} \tag{2}$$

$$S_{11}(dB) = 20 \cdot \log_{10}\left(\left|\frac{z_{in} - z_0}{z_{in} + z_0}\right|\right) \tag{3}$$

where f is the frequency the operating frequency, μ_r and ϵ_r are the relative EM parameters of the magnetic absorbing substrate, z_d is the impedance of the absorber without CR pattern.

According to the transmission line theory and the above equations, we calculate the reflection coefficients with a different a_x as illustrated in Fig. 5c and d. These results show a good agreement compared with the simulated results. To reveal the reason of the absorption characteristic with a different a_x , equivalent capacitance and inductance are calculated as depicted in Fig. 6. Figure 6a demonstrates that when a_x varies from 10 to 22 mm, the capacitance is decreased by 53% while the inductance is increased by 178%. And when the incident electric field is x -polarized, the capacitance is decreased by 63% while the inductance is increased by 357% as shown in Fig. 6b. It is obtained that the variation of a_x directly affects the equivalent capacitance and inductance,

which, therefore, determines the position of low-frequency and high-frequency absorption peak, respectively [16].

To further investigate the underlying absorption mechanism and to understand its various contributions, we computationally monitor energy dissipation in the proposed MA. The simulated energy loss density at resonance frequency is shown in Figs. 7 and 8 for the structure as a whole. We can clearly see that the electric field is mainly focused at the ends of CR along the incident electric field direction, and the strong magnetic field is mainly distributed at the left and right edges of CR but focused at the center of CR. Otherwise, according to the scale of the energy loss density, the loss at low frequency is larger than that at high frequency which demonstrates the same result for both electric loss density and magnetic loss density. Simulations reveal that the majority of energy is dissipated as magnetic loss which is an order of magnitude greater than the dielectric loss. As a result, both the electric loss and magnetic loss contribute to the broad absorption bandwidth.

Finally, the results in the above sections are all for normal incidence. But in practice, the EM wave may incident from different directions. So we first study the oblique incidence performance of the proposed absorber. Figure 9 illustrates the simulated reflection coefficients under different incident angles when the incident electric field is y - and x -polarized, respectively. From Fig. 9a, it is shown that the value of the reflection coefficient gradually increases as incident angle increases. The operation bandwidth is also reduced. When the incident angle is 30° , the -10 dB bandwidth can be achieved from 2.3 to 5.8 GHz. However, this phenomenon is different when the incident electric field is x -polarized as shown in Fig. 9b. The maximum reflection coefficient smoothly decreases and the operation bandwidth is increased when the incident angle increases to 45° , whereas the reflection coefficient increases when incident angle is larger than

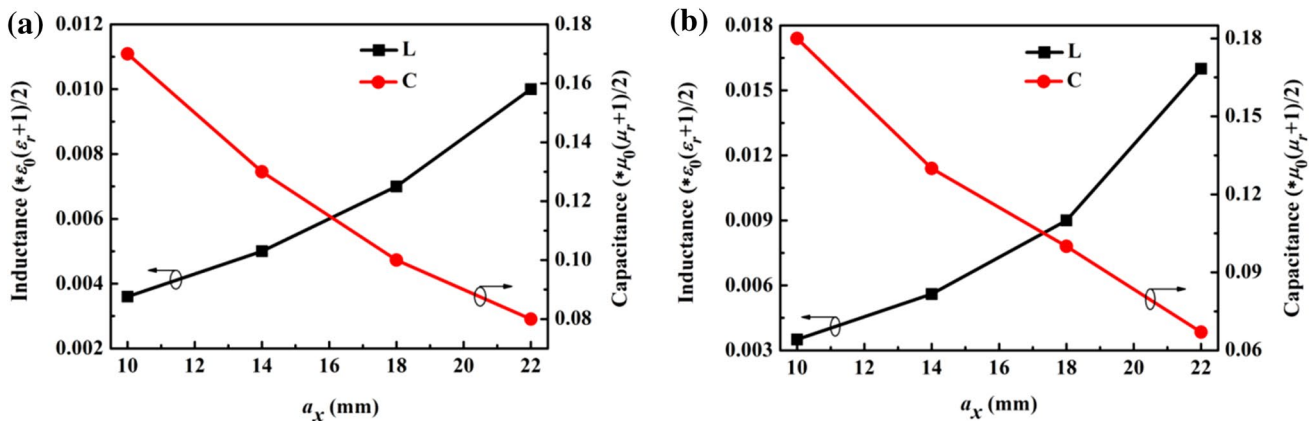


Fig. 6 The calculated results of capacitance C and inductance L for different geometrical parameter a_x when the incident electric field is **a** y -polarized and **b** x -polarized

Fig. 7 The normalized Energy loss density when incident electric field is y-polarized: electric loss density at **a** 2.5 GHz and **c** 4.8 GHz, magnetic loss density at **b** 2.5 GHz and **d** 4.8 GHz

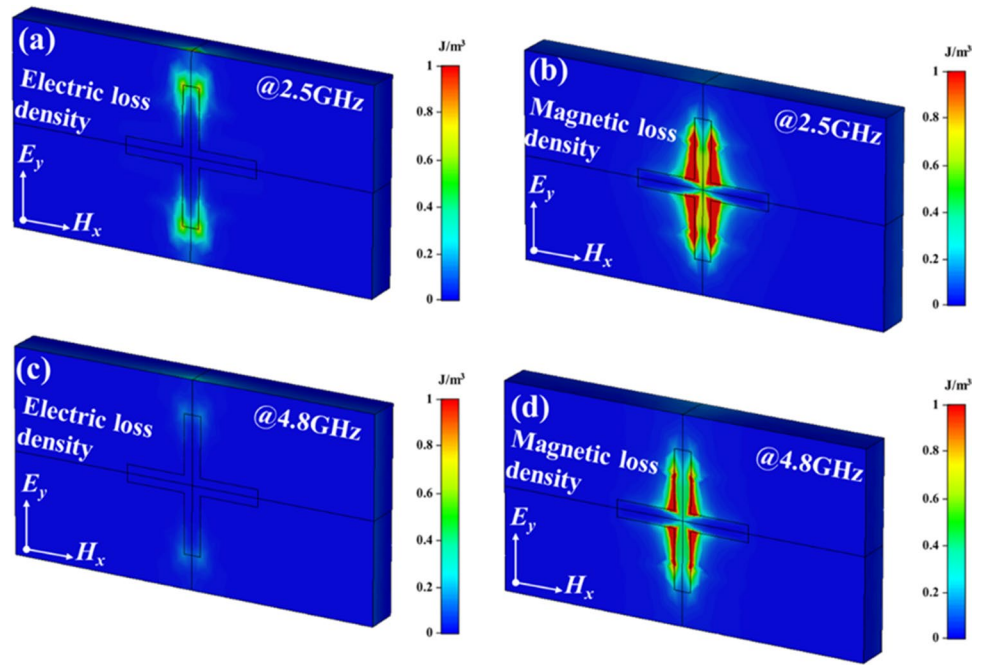
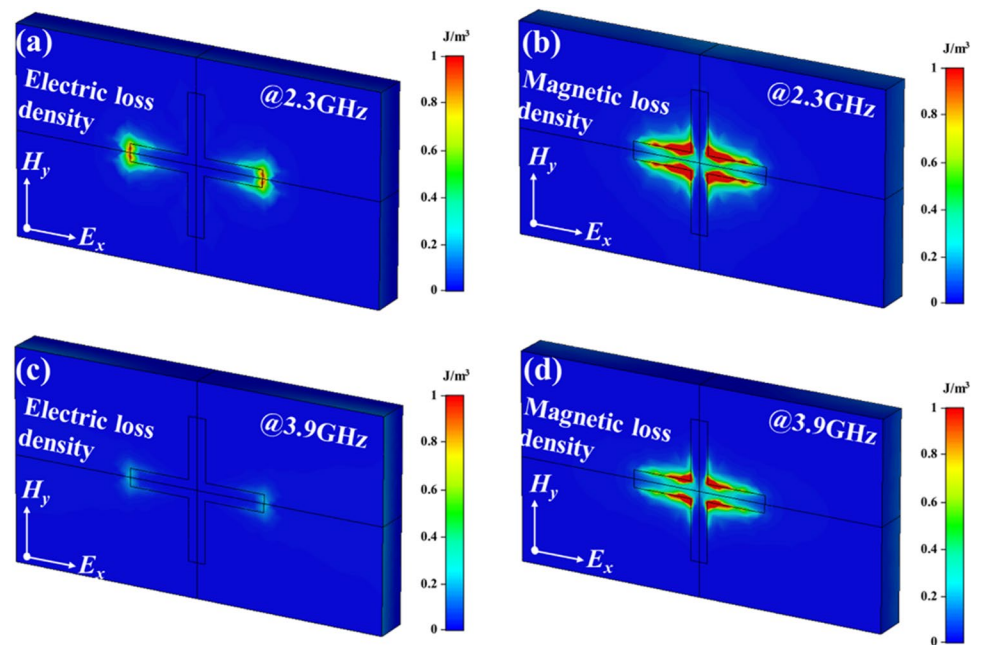


Fig. 8 The normalized energy loss density when incident electric field is x-polarized: electric loss density at **a** 2.3 GHz and **c** 3.9 GHz, magnetic loss density at **b** 2.3 GHz and **c** 3.9 GHz



60° . In this case, the -10 dB bandwidth can be achieved from 2.3 to 8.0 GHz.

Secondly, we investigate the low-frequency absorption properties of the proposed MA with different azimuth angle φ when incident angle θ is fixed under 30 degrees (angle θ and φ are defined as those formed between the propagation vector of incident waves and the z -axis over xz - and yz -plane, respectively) as shown in Fig. 10. It can be easily observed that the low-frequency resonant peak almost remains the same with the increase of azimuth

angle for both the two cases in Fig. 10. When the incident electric field is y-polarized (see in Fig. 10a) the high-frequency resonant peak tends to shift toward lower frequency, and the absorption bandwidth decreases with the increase of φ . However, the variation is different in Fig. 10b. The high-frequency resonant peak shifts toward higher frequency, and the absorption bandwidth increases with the increase of φ . When $\varphi = 90$ degrees, the absorption bandwidth can be achieved from 2.1 to 7.5 GHz.

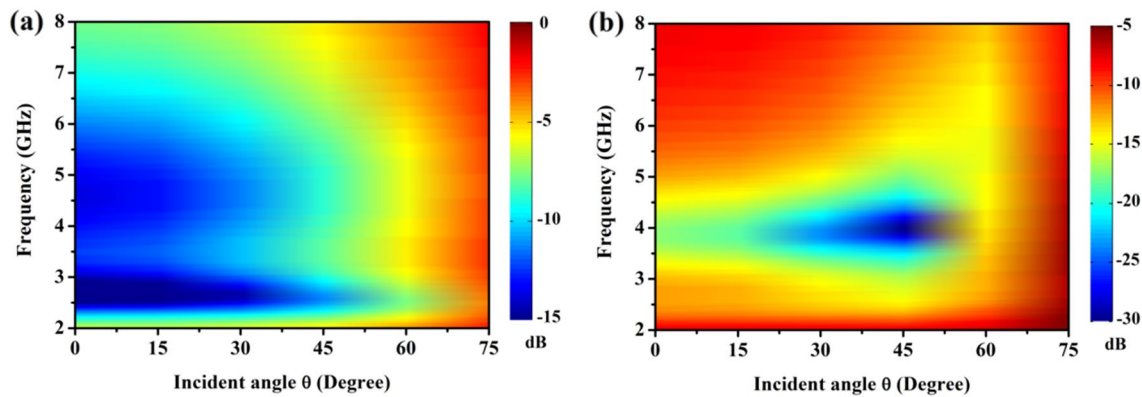


Fig. 9 Simulated reflection coefficients under different incident angle from 0° to 75° when incident electric field is **a** y -polarized and **b** x -polarized

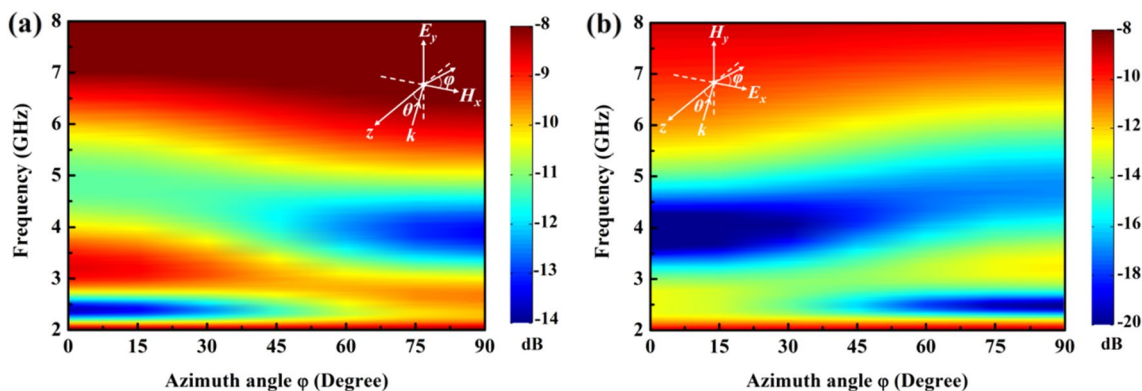


Fig. 10 Simulated reflection spectrums by varying the azimuth angle when the incident electric field is **a** y -polarized and **b** x -polarized

4 Conclusions

In this work, we have presented an ultra-thin, low-frequency and wideband magnetic-type microwave absorber. The measured results show that the proposed absorber has a low-frequency wideband strong absorption in a frequency range from 2.2 to 6.8 GHz and from 2.2 to 5.4 GHz when incident electric field is y - and x -polarized, respectively. The low-frequency absorption characteristics can be controlled based on the equivalent L - C circuit theory. The absorptive mechanism of the proposed absorber is contributed to the electric loss and magnetic loss by energy loss density. Finally, we have revealed the oblique incidence properties of the proposed absorber. The broad bandwidth can be maintained as incident angle increases up to 30 degrees for y -polarized and 60 degrees for x -polarized, respectively. Meanwhile, when the incident angle is fixed at 30 degrees and the incident field is x -polarized, the absorption bandwidth can be achieved from 2.1 to 7.5 GHz with azimuth angle of 90 degrees.

Acknowledgement This work was supported by the National Natural Science Foundation of China (Project Nos. 51025208 and 61471097), the Fundamental Research Funds for the Central Universities of China, and the Open Foundation of National Engineering Research Center of Electromagnetic Radiation Control Materials under Grant Nos. ZYGX2016K003-2.

References

1. N.I. Landy, S. Sajuyigbe, J.J. Mock et al., Perfect metamaterial absorber. *Phys. Rev. Lett.* **100**(20), 207402 (2008)
2. C.M. Watts, X. Liu, W.J. Padilla, Metamaterial electromagnetic wave absorbers. *Adv. Mater.* **24**(23), 98–120 (2012)
3. F. Ding, Y. Cui, X. Ge et al., Ultra-broadband microwave metamaterial absorber. *Appl. Phys. Lett.* **100**(10), 103506 (2012)
4. B. Wang, Y. He, P. Lou et al., Penta-band terahertz light absorber using five localized resonance responses of three patterned resonators. *Results Phys.* **16**, 102930 (2020)
5. B. Wang, G. Wang, New type design of the triple-band and five-band metamaterial absorbers at terahertz frequency. *Plasmonics* **13**(1), 123–130 (2018)
6. B. Wang, C. Tang, Q. Niu, Design of narrow discrete distances of dual-/triple-band terahertz metamaterial absorbers. *Nanoscale Res. Lett.* **14**(1), 1–7 (2019)

7. H.T. Chen, Interference theory of metamaterial perfect absorbers. *Opt. Express* **20**(7), 7165–7172 (2012)
8. N.T.Q. Hoa, T.S. Tuan, L.T. Hieu et al., Facile design of an ultrathin broadband metamaterial absorber for C-band application. *Sci. Rep.* **9**(1), 1–9 (2019)
9. Z. Zhang, L. Zhang, X. Chen, Broadband absorber for low-frequency microwave absorption in the S-band and C-band. *J. Magn. Magn. Mater.* **497**, 166075 (2020)
10. W. Yuan, Y. Cheng, Low-frequency and broadband metamaterial absorber based on lumped elements: design, characterization and experiment. *Appl. Phys. A* **117**(4), 1915–1921 (2014)
11. Y. Nie, Y. Cheng, R. Gong, A low-frequency wideband metamaterial absorber based on a cave-disk resonator and resistive film. *Chin. Phys. B* **22**(4), 044102 (2013)
12. H. Chen, H. Zhang, L. Deng, Design of an ultra-thin magnetic-type radar absorber embedded with FSS. *IEEE Antennas Wirel. Propag. Lett.* **9**, 899–901 (2010)
13. R. Huang, Z. Li, Broadband and ultrathin screen with magnetic substrate for microwave reflectivity reduction. *Appl. Phys. Lett.* **101**(15), 154101 (2012)
14. H. Zhang, L. Deng, P. Zhou et al., Low frequency needlepoint-shape metamaterial absorber based on magnetic medium. *J. Appl. Phys.* **113**(1), 013903 (2013)
15. Y. Cheng, Y. Nie, X. Wang et al., Adjustable low frequency and broadband metamaterial absorber based on magnetic rubber plate and cross resonator. *J. Appl. Phys.* **115**(6), 064902 (2014)
16. L. Zhang, P. Zhou, H. Zhang et al., A broadband radar absorber based on perforated magnetic polymer composites embedded with FSS. *IEEE Trans. Magn.* **50**(5), 1–5 (2014)
17. D. Huang, F. Kang, C. Dong et al., A second-order cross fractal meta-material structure used in low-frequency microwave absorbing materials. *Appl. Phys. A* **115**(2), 627–635 (2014)
18. L. Zhang, P. Zhou, H. Chen et al., Ultra-thin wideband magnetic-type metamaterial absorber based on LC resonator at low frequencies. *Appl. Phys. A* **121**(1), 233–238 (2015)
19. J. Lim, Y. Ryu, S. Kim, Dual-band microwave absorption properties of metamaterial absorber composed of split ring resonator on carbonyl iron powder composites. *Electron. Mater. Lett.* **11**(3), 447–451 (2015)
20. W. Li, X. Qiao, Y. Luo et al., Magnetic medium broadband metamaterial absorber based on the coupling resonance mechanism. *Appl. Phys. A* **115**(1), 229–234 (2014)
21. P.H. Zhou, L.J. Deng, J.L. Xie et al., Effects of particle morphology and crystal structure on the microwave properties of flake-like nanocrystalline Fe₃Co₂ particles. *J. Alloy. Compd.* **448**(1), 303–307 (2008)
22. T. Liu, P.H. Zhou, J.L. Xie et al., Extrinsic permeability of Fe-based flake composites from intrinsic parameters: a comparison between the aligned and random cases. *J. Magn. Magn.* **324**(4), 519–523 (2012)
23. L.F. Chen, C.K. Ong, C.P. Neo et al., *Microwave Electronics-Measurement and Material Characterization* (John Wiley and Sons, England, 2004)
24. N. Marcuvitz, *Waveguide handbook* (Peter Peregrinus Ltd, London, 1986), pp. 280–284
25. J. Zhou, Unifying approach to left-handed material design. *Opt. Lett.* **31**(24), 3620–3622 (2006)
26. B. Wang, G. Wang, L. Wang, Design of a novel dual-band terahertz metamaterial absorber. *Plasmonics* **11**, 523–530 (2016)
27. B. Wang, G. Wang, T. Sang, Simple design of novel triple-band terahertz metamaterial absorber for sensing application. *J. Phys. D Appl. Phys.* **49**(16), 165307 (2016)

Publisher's Note Springer Nature remains neutral with regard to jurisdictional claims in published maps and institutional affiliations.